ACS OMEGA

http://pubs.acs.org/journal/acsodf

Article

# Electrochemical Sensing of Roxarsone on Natural Biomass-Derived Two-Dimensional Carbon Material as Promising Electrode Material

Nikhil, S. K. Srivastava, Amit Srivastava, Monika Srivastava,* and Rajiv Prakash*

Cite This: *ACS Omega* 2022, 7, 2908−2917

Read Online

ACCESS | Metrics & More | Article Recommendations

**ABSTRACT:** Herein, we report the electrochemical detection of roxarsone (ROX) on a two-dimensional (2D) activated carbon (AC)-modified glassy carbon electrode (GCE). Meso/microporous 2D-AC is synthesized from a natural biomass Desmostachya bipinnata, commonly known as Kusha in India. This environment-friendly material is synthesized by chemical activation using potassium hydroxide (KOH) and used as a sensitive electrochemical platform for the determination of ROX. It is an arsenic-based medicine, also used as a coccidiostat drug. It is widely used in poultry production as a feed additive to increase weight gain and improve feed efficiency. Long-term exposure to arsenic leads to serious health problems in humans and demands an urgent call for sensitive detection of ROX. Therefore, the green synthesis of 2D-AC is introduced as new carbon support for the electrochemical sensing of ROX. It provides a large surface area and efficiently supports enhanced electron transfer. Its electrocatalytic activity is seen in potassium ferri/ferrocyanide by cyclic voltammetry, where the 2D-AC-modified GCE delivered five to six times higher electrochemical performance as compared to the unmodified GCE. Electrochemical impedance spectroscopy is also performed to show that the prepared material has faster electron transfer and permits a diffusion-controlled process. It works well in real samples and also on disposable screen-printed carbon electrodes, thereby showing great potential for its application in clinical diagnosis. Our results exemplify a modest and innovative style for the synthesis of excellent electrode material in the electrochemical sensing platform and thus offer an inexpensive and highly sensitive novel approach for the electrochemical sensing of ROX and other similar drugs.

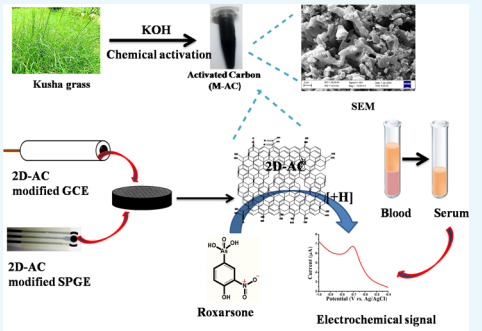

Electrochemical Sensor for arsenic based drug Roxarsone from Kusha grass derived 2D-Activated Carbon over GCE / SPGE and in Real sample by DPV

## 1. INTRODUCTION

Organic arsenic, a less toxic form of arsenic present in the form of roxarsone (ROX) (3-nitro-4-hydroxyphenyl arsonic acid) as an enhanced animal drug used for the treatment of parasitic disease coccidiosis, could be converted into inorganic arsenic.[1,2] It is also injected in chicken that is bred specifically for meat consumption in poultry farming.[3,4] Chickens that consumed roxarsone-containing feed (20−40 mg $kg^{-1}$) demonstrated arsenic concentrations of 3−7, 2−5, and 2−6 $\mu g\ kg^{-1}$ in the liver, muscle, and heart, respectively.[5] Many of the arsenic compounds released from animal waste are water-soluble, thereby increasing inorganic arsenic in the environment and causing contamination. Acceptable levels of arsenic in different countries range from 50 to <10 ppb in drinking water. In addition, the consumption of roxarsone in meat must be 5.0−6.0 mg $Kg^{-1}$. Higher concentrations of arsenic are closely related to serious cancer toxicity in humans.[6−8] Long-term arsenic exposure also implies cardiovascular diseases,[9] neurological disorders,[10] diabetes,[11] birth-related issues,[12] and endocrine disorders.[13] Therefore, a profound diagnosis of roxarsone has attracted increasing attention from researchers in food analysis and in human health-oriented platforms. Electrochemical methods are widely used in the detection of several feed additives, as they have low costs, good sensitivity and selectivity, and rapid detection and portability.[14−18] However, there are a few reports in which electrochemical sensing is performed for the detection of ROX.[19−21]

Carbon-based materials have attracted immense attention as electrode materials because of their high electrical conductivity, specific microstructure, and good stability. Such carbon materials can be engineered for good sensitivity and selectivity.[22−26] Apart from several graphene or CNT-like materials, it is also important to explore environment-friendly, efficient, and cost-effective carbon materials for several applications. Toward this end, biomass-derived activated carbon materials have been attracting competent interest due to their high surface area, less toxicity, adjustable pore size, good electrical conductivity, chemical stability, and the presence of heteroatoms that provide good functionality.[27−29]

**Received:** October 16, 2021
**Accepted:** December 29, 2021
**Published:** January 11, 2022

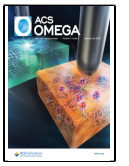

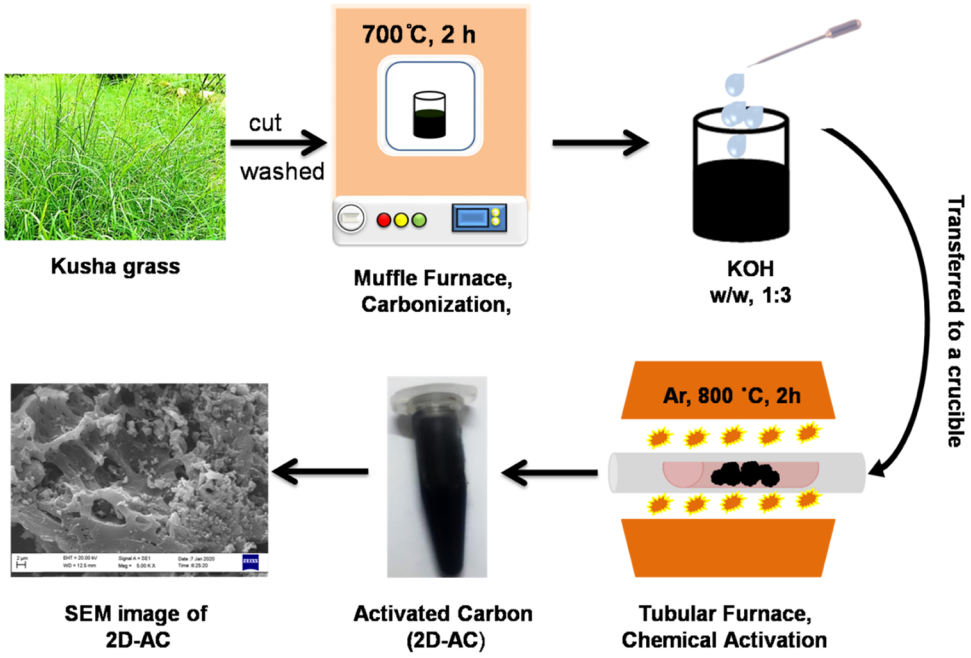


**Figure 1.** Schematic representation of two-dimensional activated carbon.

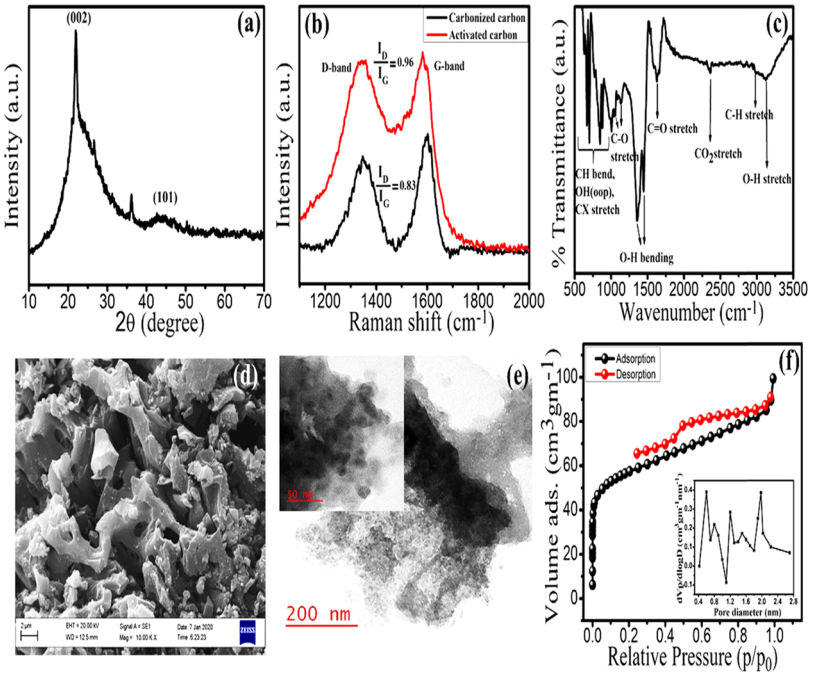


**Figure 2.** Characterization of two-dimensional (2D) activated carbon using (a) XRD, (b) Raman (before and after activation) (c) Fourier transform infrared (FTIR) spectroscopies, (d) scanning electron microscopy (SEM), and (e) high-resolution transmission electron microscopy (HR-TEM) image; the inset shows an enlarged view of the TEM image. (f) $N_2$ adsorption−desorption isotherms; the inset shows the pore size distribution curve.

Activated carbon is a carbon-containing solid that is obtained from biomass, biochar, coal, lignite, and petroleum pitch, using pyrolysis. In the process, a carbon material is processed for increased surface area, allowing it to absorb a larger quantity of molecules and chemical reactions. The large surface area of activated carbons results in a greater amount of porosity. The activation can be performed by either physical or chemical activation processes. In physical activation, the precursor is pyrolyzed in the 600−1200 °C range in an inert atmosphere, and the obtained carbonized product is activated by $CO_2$[30] and steam.[31] While in chemical activation, alkali and metal salts such as $MgCl_2$,[32] $K_2CO_3$,[33] KOH,[34] $Na_2CO_3$,[35] NaOH,[36] $ZnCl_2$,[37] and $H_3PO_4$[38] are used along with precursors, and the obtained product is pyrolyzed in the 400−950 °C range. The synthesis of activated carbon is simple, environment-friendly, and economical. Very recently, eragrostis cynosuroids (grass family) was used as a source of activated carbon for energy storage devices using $ZnCl_2$ as an activating agent.[39] Activated carbons have been used in several applications such as Li-ion batteries,[40] sensors,[41−43] super-



https://doi.org/10.1021/acsomega.1c05800
ACS Omega 2022, 7, 2908−2917

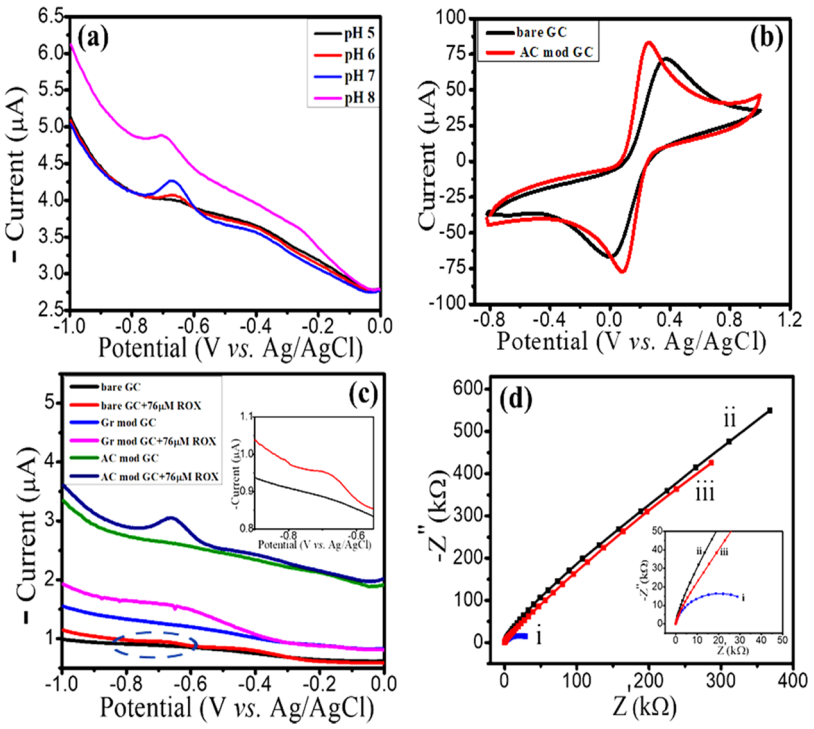


**Figure 3.** (a) Study of different pH values using DPV; (b) CV plot of bare and 2D-AC-modified GCE in 5.0 mM $K_3[Fe(CN)_6]/K_4[Fe(CN)_6]$ redox couple in 0.1 M PBS at the scan rate of 50 mV $s^{-1}$; (c) DPV plot of bare GCE, graphite powder (Gr)-modified GCE, and 2D-AC-modified GCE in 0.1 M PBS at pH 7 in the absence and presence of 76 $\mu$M ROX (the inset shows an enlarged view of the dotted circled area); and (d) the Nyquist plots of (i) bare GCE, (ii) 2D-AC without ROX, and (iii) 2D-AC-modified GCE with 76 $\mu$M ROX.

capacitors,[44] removal of toxic metal ions and organic dyes,[45] and electrocatalysts;[46] however, their application in electrochemical sensing is not extensive.

In the present study, meso/microporous activated carbon (2D carbon) was prepared from natural biomass Kusha grass (Desmostachy abipinnata) using KOH as an activating agent, which enhances further the adsorption capacity of the exposed surface for metal adsorption. Desmostachya bipinnata belongs to the grass family, Poaceae. The motivation behind choosing Kusha grass was that the rate of production of such agricultural waste including grass, leaves, and flowers is very high in India. These materials have high lignin and cellulose contents containing carboxylic and phenolic polar functional groups, which also have a metal-binding ability.[47−49] The present study provides a first-of-its-kind allocation with the fabrication of highly electroactive surface areas for electrode modification using biowaste. Till now, no literature reports have been available for the sensing of toxic drug ROX on this biowaste-derived activated carbon (2D carbon) for the modification of commercial electrodes using the differential pulse voltammetry (DPV) method. Hence, we deal with such abundant biomass-derived activated carbon, which has no toxicity, is environment-friendly, and provides an economical alternative option as a new electrode material for electrochemical sensing. However, earlier reports available for the electrochemical sensing of ROX have used hazardous toxic chemicals for electrode material preparation.

## 2. RESULTS AND DISCUSSION

**2.1. Characterization of Activated Carbon.** The X-ray diffraction (XRD) pattern of the prepared 2D carbon in Figure 2a shows two characteristic peaks of any activated carbon. Peaks at 22 and 43.5° correspond to (002) and (101) planes, respectively. The (002) peak is broad at the base and sharp at the top containing both the amorphous and crystalline nature of graphitic carbon and indicating the presence of a few single exfoliated layers.[50] The peak at 43.5° is ascribed to the creation of pores due to decomposition of the carbon ring in the direction of the graphitic arrangement and formation of more organized aromatic carbon. Such a newly formed structure was more stable than the amorphous carbon only (Figure 1 shows schematic representation for the synthesis of 2D-AC).

Raman spectra after carbonization and activation are shown in Figure 2b. The two strong peaks displayed in the spectra correspond to the D-band and G-band, respectively. In activated carbon, the G-band is broad and occurs at 1580 $cm^{-1}$, relating to the first-order Raman band of the $sp^2$-bonded graphitic region. Also, the peak at 1345 $cm^{-1}$, which corresponds to the D-band, occurs because of amorphous carbon (disordered), grain boundaries, and size reduction of the $sp^2$-bonded carbon network.[51] The intensity ratio of D and G bands is used to determine the degree of $sp^2$ ordering in carbon materials. It is found that after activation, the $I_D/I_G$ value representing the disorderness is considerably more than that of the carbonized sample (from 0.83 to 0.96), signifying that the activation process allowed for activated carbon (AC) to have more defective sites upon thermal reduction.[52]

Kusha grass contains a high content of organic components such as lignin and cellulose and various types of polar functional groups such as phenolic and carboxylic acids. The FTIR spectrum shown in Figure 2c depicts a broad adsorption peak at around 3150 $cm^{-1}$, which may be due to the presence of intermolecular hydrogen bonding in hydroxyl, O−H in phenolic, carboxylic, and alcoholic groups. The small peak at 2930 $cm^{-1}$ is attributed to the C−H stretching in CH, $CH_2$, and $CH_3$ groups. The peak at 2350 $cm^{-1}$ may be assigned to


https://doi.org/10.1021/acsomega.1c05800
ACS Omega 2022, 7, 2908−2917

C═O stretching in $CO_2$, which may be adsorbed on surface-activated carbon. The prominent band at 1630 $cm^{-1}$ occurs due to the C═O stretching in carbonyl groups. The peaks at around 1450 and 1355 $cm^{-1}$ are due to the O−H bending vibration and 1130−1060 $cm^{-1}$ is due to the C−O stretching vibration. While the peaks from 630 to 1000 $cm^{-1}$ can be attributed to C−H deformation in alkynes, 5C−H bending (out of plane) in alkenes, C−H bending and ring crumpling in arenes, O−H bending (out of plane), and C−X stretching of halo compounds.[53]

The surface morphology of as-prepared 2D carbon was first investigated using scanning electron microscopy, as shown in Figure 2d. Foam or spongelike defects on the surface having several pores of different sizes can be observed. It also describes that such irregularities were developed during the activation process. The bigger size was probably due to sample preparation, where the powder form of AC was taken, which becomes agglomerated.

Further, transmission electron microscopy was also performed to observe the structure of the prepared sample. Figure 2e shows the interconnected pores formed inside the 2D carbon sheets. This may be due to the evolution of gases during carbonization. The dispersed sample was used in this characterization, where the nanometer-sized material formation was justified.

The porosity nature of as-synthesized activated carbon was examined using $N_2$ adsorption−desorption isotherms, as shown in Figure 2f. The figure shows type IV nitrogen adsorption isotherms where the black line shows $N_2$ adsorption while the red line represents its desorption. The red line did not follow the path of the black line and formed a looplike structure between 0.45 and 0.95 relative pressures ($P/P_0$). Such features advocated the occurrence of micro- and mesopores in the sample. The creation of this loop indicates that 100% $N_2$ was not released and trapped in the small pores present in the AC. The inset of this figure shows the corresponding pore size distributions obtained from the Barrett−Joiner−Halenda (BJH) method, which also emphasized the presence of micro- and mesopores (0.4−2.8 nm), where the average pore diameter was found to be 1.79 nm. The specific surface area of the as-synthesized AC was found to be 194 $m^2\ g^{-1}$. The presence of such a small pore diameter offered a good corridor for strong adsorption of the target analyte and further led to enhanced electrochemical performance and high sensitivity of 2D carbon as suitable electrode material for sensing.[54,55]

## 3. ELECTROCHEMICAL STUDIES

**3.1. Effect of pH and a Comparative Study of Differently Modified Electrodes.** Glassy carbon electrode was chosen and modified with the prepared activated carbon for this particular study; then, the electrochemical performance of ROX at the AC modified glassy carbon electrode (GCE) was investigated using DPV with pH values of 5, 6, 7, and 8 for obtaining optimal conditions to obtain high peak currents and well-defined peak shapes. The results are shown in Figure 3a. It can be seen that the cathodic peak current increases from 5 to 7 and thereafter decreases. Also, the peak potential shifts to a more negative value from pH 5 to 8. Additionally, pH 7.0 is more stable and shows a better response; therefore, we can choose a phosphate-buffered saline (PBS) solution of pH 7.0 for subsequent electrochemical experiments.[20]

Furthermore, the electrochemical behavior of bare and AC-modified GCE was studied in potassium ferrocyanide/potassium ferricyanide (Fe(II)/Fe(III)) redox couple. Results obtained are shown in Figure 3b, where peaks of 2D carbon-modified GCE were shifted toward lower potential as compared to bare GCE in the presence of the redox probe $K_3[Fe(CN)_6]/K_4[Fe(CN)_6]$ in 0.1 M PBS with current enhancement, which was attributed to the rapid electron transfer kinetics with a superior electroactive surface area of the modified electrode. This shifting of potential clearly indicated the catalytic behavior of the prepared material.

The electrochemical behavior of the prepared 2D carbon was also determined in 0.1 M PBS only (pH 7) with and without ROX at both bare and modified GCE, as shown in Figure 3c. The figure depicts that addition of 76 $\mu$M ROX over bare GCE did not show a clear change, while 2D carbon-modified GCE gave a significant reduction peak at 0.66 V in DPV. Also, the efficiency of synthesized AC is compared and validated on commercially available graphite powder (Gr)-modified GCE with and without ROX. It was also evident from Figure 3c that the Gr-modified GCE did not give a well-resolved peak with our analyte roxarsone. Such superior nature of as-synthesized 2D-AC may be because of its big porous structure bestowing a large surface area, excellent conductivity, and rapid mass and electron transfer. In all cases, the signature was observed almost at the same potential. To validate the effect of surface area, the electrochemical active surface area (EAS) was calculated using Randles−Sevick equation[56] by cyclic voltammetry technique in 5.0 mM $K_3Fe(CN)_6/K_4Fe(CN)_6$ as a test solution in 0.1 M PBS buffer, at different sweep rates and $T$ = 298 K for bare GCE, Gr-modified GCE, and AC-modified GCE as follows

$$I_p = 2.69 \times 10^5 \times A \times D^{1/2} n^{3/2} \nu^{1/2} C$$

where $A$ is the area of the electrode surface, $D$ is the diffusion coefficient, i.e., $7.6 \times 10^{-6}$ $cm^2\ s^{-1}$, $\nu$ is the sweep rate (mV $s^{-1}$), and $C$ is the concentration of $K_3Fe(CN)_6/K_4Fe(CN)_6$ redox couple in the electrolyte. From the slope of the plot of $I_p$ vs $\nu^{1/2}$, the approximate value of the surface area of the bare GC electrode, graphite-modified GCE, and AC-modified GCE was found to be 0.052, 0.065, and 0.075 $cm^2$, respectively.

The above findings lead us to perform a comparison of charge transfer behavior between the reference electrode (RE) and the vicinity of bare and modified electrodes (usually called a working electrode, WE) using electrochemical impedance spectroscopy (EIS). EIS was performed at their open-circuit potentials (OCPs) within a frequency range from 0.01 Hz to 100 KHz with an AC amplitude of 5 mV at room temperature. EIS analysis shows the behavior of the glassy carbon (GC) electrode surface and determines the interfacial properties of 2D carbon over it. Figure 3d shows the Nyquist plot of the bare and modified GCEs with and without 76 $\mu$M drug in 0.1 M PBS buffer solution at pH 7. The inset shows the zoomed-in part of the same Nyquist plot. A general explanation of the EIS plot depicts that if the formation of the semicircle is inclined to the $Z'$-axis and/or linked with a straight line at about a 45° angle, then it is said to be the outcome of resistance to charge transfer between working and reference electrodes with diffusion-dominated mass transfer in the surrounding area of the working electrode.[57] Similarly, it is also reported and demonstrated in the literature that inclination of the straight


https://doi.org/10.1021/acsomega.1c05800
ACS Omega 2022, 7, 2908−2917

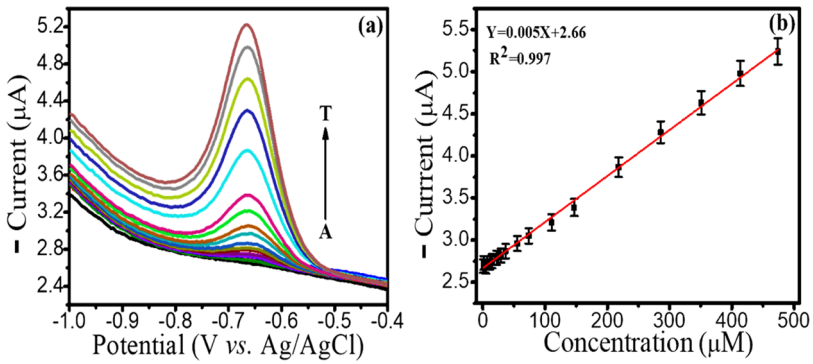


**Figure 4.** DPV curve (a) and its calibration plot (b) of 2D carbon-modified GCE with successive addition of ROX (0 $\mu$M, then 0.76−474 $\mu$M) in deoxygenated 0.1 M PBS (pH 7.0) at 50 mV $s^{-1}$.

line toward the Z'-axis expresses more charge accumulation on the working electrode as compared to its counter ones.[58] From Figure 3d, curves "ii" and "iii" are more inclined toward the Z'-axis as compared to curve "i" showing more charge accumulation on the electrode surface and favoring a diffusion-dominated phenomenon. However, on comparing curves "ii" and "iii", it was observed that after addition of 76 $\mu$M ROX, curve "iii" was inclined toward the Z'-axis, creating more resistance as some active sites on the modified electrode were now covered by the analyte moiety. Hence, 2D carbon shows efficient electrical communication at the electrode surface.

**3.2. Electrocatalytic Reduction of Roxarsone over GCE.** Differential pulse voltammetry was applied to discuss the catalytic nature of 2D carbon-modified GCE for different concentrations of the toxic drug ROX. In Figure 4a, ROX showed a reduction peak at −0.66 V. The entire study was performed in the −0.4 to −1.0 V potential range, and the study was conducted in a linear range of 0.76−474 $\mu$M (there was saturation beyond 474 $\mu$M, observed at 549.62 $\mu$M). From the figure, it is evident that the cathodic peak or reduction peak for ROX increases excellently with an increasing concentration of ROX at 2D carbon-modified GCE. 2D carbon permitted better electron transfer on the surface of GCE and showed an extremely good linear response toward ROX, as shown in Figure 4b. The experiment was carried out in triplicate. However, error bars were added by calculating current variations in each set of experiments at a fixed concentration of ROX. This nonenzymatic electrochemical sensor exhibits a good sensitivity of 0.0714 $\mu A \cdot \mu M^{-1} \cdot cm^{-2}$ with $R^2$ = 0.997. Then, the limit of detection (LOD) was measured by back extrapolation of the linear fit line on the Y-axis and calculated to be 1.5 nM, whereas the LOQ (limit of quantification) was 0.76 $\mu$M.

Table 1 shows comparative analytical performance toward ROX with a few previously reported research articles. However, we found that very few reports in the literature were related to the electrochemical method. Additionally, the proposed electrochemical reaction mechanism is shown in Figure 5, describing the reduction of ROX in the presence of 2D carbon-modified GCE. It demonstrates the electro-reduction of $NO_2$ to NH−OH, which occurs at −0.66 V and undergoes an irreversible reduction process as there is no anodic peak observed in CV.[19,20]

**3.3. Validation in Real Samples.** These observations lead us to perform subsequent experiments in real samples under the above-mentioned conditions. Therefore, the practical

**Table 1. Comparison of the Analytical Performance of ROX with Other Published Studies**

| technique | LOD (nM) | linearity ($\mu$M) | matrix/sample | reference |
|---|---|---|---|---|
| DPV | 30 | 0.05−490 | phosphate buffer | 19 |
| DPV | 75 | 0.1−442.6 | phosphate buffer | 20 |
| amperometric method | 22.5 | 0.035−1816.5 | phosphate buffer | 21 |
| DPV | 1.5 | 0.76−474 | phosphate buffer | our work |
| | 1.8 | 5.31−23.55 | blood serum | our work |

applicability of 2D carbon-modified GCE was determined in a human blood serum sample using the same DPV technique. The sample was diluted with PBS buffer in a 1:10 ratio. Then, the prepared solution was spiked with different known concentrations of ROX and analyzed using DPV under the same optimized conditions as shown in Figure 6. It was evident from the figure that the cathodic current increases linearly from 5.31 to 23.55 $\mu$M. Moreover, the cathodic peak current values were plotted against the concentration of ROX to obtain a straight line with $R^2$ = 0.984. The developed sensor proved its efficiency for use with good sensitivity of 0.571 $\mu A \cdot \mu M^{-1} \cdot cm^{-2}$, LOQ of 5.31 $\mu$M, and LOD of 1.8 nM.

Thereafter, the reduction of ROX was also validated over commercially available and disposable screen-printed carbon electrode (SPCE), which was a ready-to-use electrode as shown in Figure 7. SPCE modification was carried out as discussed under the experimental section. The figure showed regular enhancement in cathodic current peak with increasing concentration of ROX. Figure 7b shows its corresponding calibration plot having good linearity with $R^2$ = 0.978 with 0.0519 $\mu A \cdot \mu M^{-1} \cdot cm^{-2}$ sensitivity. Here, LOD obtained was 5.17 nM, whereas LOQ was 1.89 $\mu$M.

**3.5. Reproducibility and Storage Stability Test.** Keeping all parameters the same, electrode modification was carried out in four sets. Then, the corresponding DPV in 0.1 M PBS with 76 $\mu$M ROX was performed, and it was found that all of the four curves almost coincided with each other, suggesting good reproducibility of the prepared sensor. Figure 8a shows up to 97% retention in current. Further, the storage ability of the as-developed sensor was tested for 1 month. Figure 8b shows the DPV curve on the first day and after its thirtieth day, whereas its inset showed percentage current retention at an interval of 3 days for the next 30 days. The bar graph showed excellent stability up to 30 days with little attenuation in


https://doi.org/10.1021/acsomega.1c05800
ACS Omega 2022, 7, 2908−2917

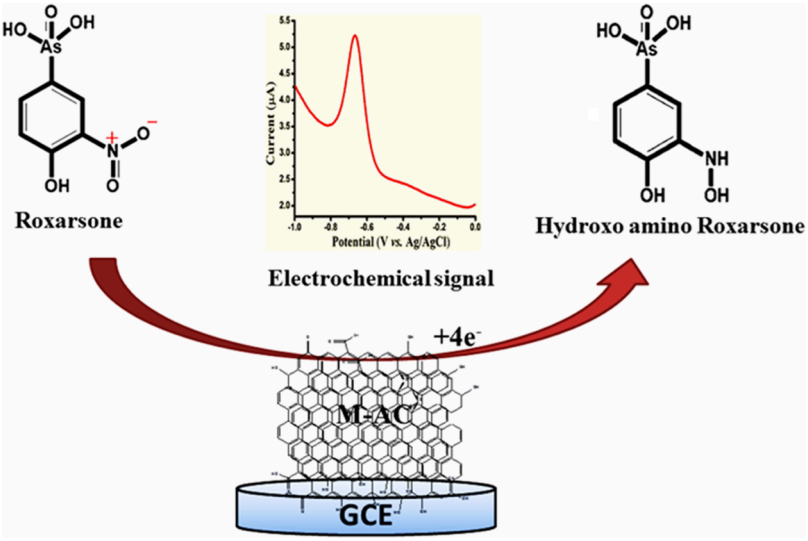


**Figure 5.** Schematic representation of the reduction of roxarsone on 2D carbon-modified electrode.

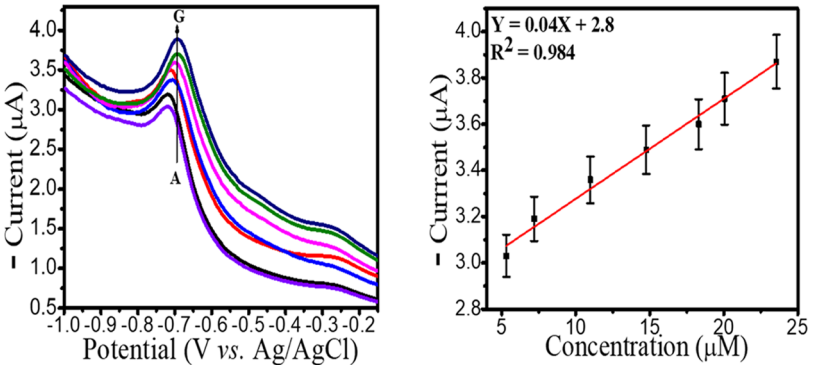


**Figure 6.** DPV curve and its calibration plot of 2D-AC-modified GCE with successive addition of ROX (5.31−23.55 $\mu$M) in deoxygenated 0.1 M PBS (pH 7.0) in human blood serum at a 50 mV $s^{-1}$ scan rate.

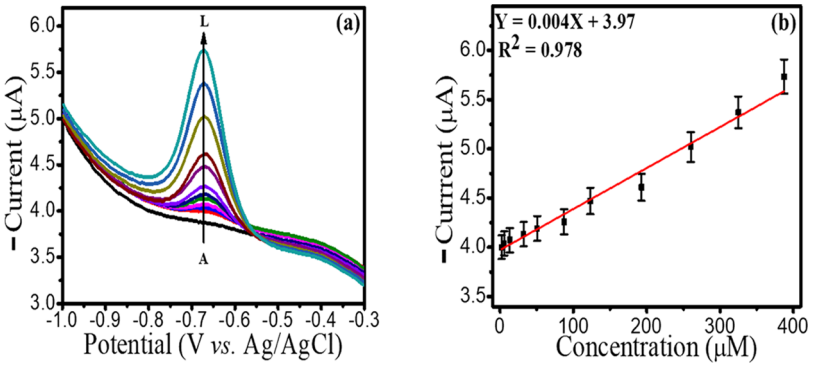


**Figure 7.** DPV curve (a) and its calibration plot (b) of M-AC-modified SPCE with successive addition of ROX (1.89−387.34 $\mu$M) in deoxygenated 0.1 M PBS (pH 7.0) at 50 mV $s^{-1}$.

current when stored at ambient temperature. During storage, no extraordinary condition was maintained, and it was found that about 95% current was retained even after 1 month. It can be visualized from these findings that the proposed sensing platform can be safely used for a month or more than that with good accuracy for the detection of ROX.

**3.6. Study of Interference.** To explore further the selectivity of 2D carbon-modified electrode toward ROX sensing, several interferents were added along with ROX, and the results were investigated in percentage change in the cathodic current in DPV in the presence of 0.1 M PBS (pH 7). The concentration of all interferents ($Na_2S$, $NO_2^-$, $NO_3^-$, D-glucose, paracetamol tablet, ascorbic acid, and folic acid) was taken to be 10 times higher than that of ROX. Results shown in Figure 9 depict that 2D carbon-modified electrode was able to anti-interfere with roxarsone even with much higher concentrations of interferents in this electrochemical sensing and was fit for use in biological samples. The most probable reason for this selectivity is that AC exhibited a high adsorption capacity for ROX, which was presumably attributed


https://doi.org/10.1021/acsomega.1c05800
ACS Omega 2022, 7, 2908−2917

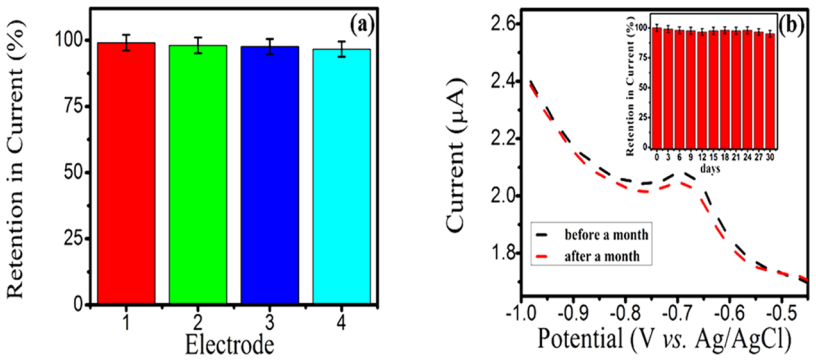


**Figure 8.** (a) Reproducibility and (b) storage stability test of 2D carbon-modified electrode using DPV in the presence of 76 $\mu$M ROX in 0.1 M phosphate buffer (pH 7). The inset shows % current retention in the interval of 3 days.

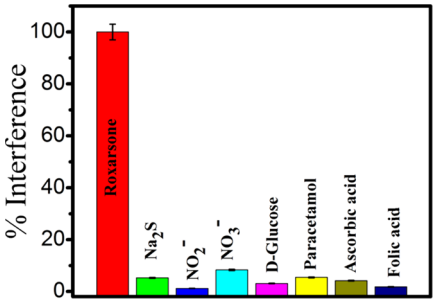


**Figure 9.** Interference study using various biological compounds toward ROX in a 10:1 ratio in 0.1 M phosphate buffer (pH 7).

to the interaction of electrostatic attraction, hydrogen bonding, and $\pi-\pi$ interaction between the adsorbent and the adsorbate.[59] Also, in voltammetry scans, biomolecules and drugs show no peak response or no reduction peak in the region where ROX shows reduction.

## 4. CONCLUSIONS

In summary, we proposed the synthesis of meso/microporous activated carbon as a sustainable, eco-friendly, and easy-to-employee material for electrode modification and further use it for the electrochemical sensing of arsenic-based medicine ROX through DPV. The as-prepared 2D carbon was characterized using XRD, Raman and FTIR spectroscopies, TEM, and SEM. The meso/microporous nature of AC was validated using $N_2$ adsorption−desorption isotherms and BET analysis with a specific surface area of 194 $m^2\ g^{-1}$. The performance of the as-synthesized 2D carbon was also validated with commercially available graphite powder for electrode modification. The superiority of 2D-AC was proved by comparing its EAS value with Gr-modified GCE and bare GCE as 0.075, 0.065, and 0.052 $cm^2$, respectively. 2D carbon showed excellent electro-catalytic behavior based on an enzyme-free sensor for the detection of the toxic drug roxarsone. Under optimum conditions, the ROX sensor is designed and developed and works well at −0.66 V (vs Ag/AgCl). Specific features of the proposed sensor include a wide linear series (0.76−474 $\mu$M) with a detection limit in the nanomolar range (1.5 nM) and good sensitivity (0.0714 $\mu A{\cdot}\mu M^{-1}{\cdot}cm^{-2}$) on glassy carbon electrode. 2D carbon-modified electrodes have been effectively applied in human blood serum samples toward the determination of ROX (LOD = 1.8 nM). They work well with screen-printed carbon electrodes (SPCEs), also showing reliable sensitivity and LOD. Results show a potential to be used as an electrochemical platform for the catalyzing ability of economically synthesized 2D carbon toward ROX (toxic arsenic-based antibiotic medicine) in real samples with a good recovery rate using DPV. The as-synthesized 2D-AC proves itself as a promising electrode material and may be apprehended in a short time. The developed sensor is validated for selectivity, storage stability, and reproducibility toward ROX. These findings recommend it as a promising method for sensing ROX electrochemically for arsenic-based chemical detection.

## 5. EXPERIMENTAL SECTION

**5.1. Reagents.** Roxarsone was bought from Sigma-Aldrich. Kusha grass was locally collected from the Banaras Hindu University campus. Other chemicals used such as potassium hydroxide (KOH) and HCl were procured from Merck, India. The solutions were prepared using deionized (DI) water (Millipore Q system), and for electrochemical studies, aqueous solutions were purged using high-purity nitrogen gas for 15 min before the experiment. Each experiment was performed at ambient temperature, i.e., 25 °C.

Human blood serum was collected from blood donor volunteers of the institute (courtesy: Institute of Medical Sciences, BHU, Varanasi), and methods were followed in accordance with relevant guidelines and regulations.

**5.2. Synthesis of 2D-Activated Carbon.** Kusha grass was collected locally and cut into small pieces. Thereafter, it was washed four to five times with DI water. Cleaned Kusha grass was then kept at 100 °C in a vacuum oven for drying. Next, carbonization was performed at 700 °C for 2 h in a muffle furnace at a 5.8 °C $min^{-1}$ heating rate. Then, it was crushed into a powder and then mixed with KOH w/w in a 1:3 ratio for its chemical activation. Mortar and pestle were used to make a homogeneous mixture. Further, DI water was added to this mixture, and this aqueous solution was kept under normal stirring overnight. The as-obtained slurry was transferred to a crucible and kept in a tubular furnace under an inert argon atmosphere at 800 °C for 2 h again at a 5.8 °C $min^{-1}$ heating rate. It was then allowed to cool to normal temperature, washed with dilute HCl until it reached pH 7, filtered, and finally kept in a vacuum oven for complete drying (Figure 1).

**5.3. Fabrication of 2D-Activated Carbon-Modified Electrode.** Glassy carbon electrode (GCE) was cleaned using alumina slurry (0.05 mm) followed by ultrasonication in ethanol and then distilled water for 10 min each. Further, for modification of GCE (3 mm disc diameter) with activated carbon, an aqueous solution of the activated carbon (1 mg


https://doi.org/10.1021/acsomega.1c05800
ACS Omega 2022, 7, 2908−2917

$mL^{-1}$ in distilled water) was prepared, cast over GCE, and dried in a vacuum desiccator. No binder was used for electrode fabrication because the synthesized activated carbon adsorbed well on commercial GCE, which was validated by running a CV scan for several cycles to observe any material loss for a particular set of conditions (data not shown). It was observed that the initial scan did not trace the path because of diffusion; however, later scans traced the path exactly, showing no material loss. The same procedure is repeated for SPCE, except for its cleaning.

**5.4. Instrumentation.** X-ray diffraction was performed on a Miniflex 600 diffractometer, using Cu K$\alpha$ (K$\alpha$ = 1.54056 Å) radiation. The morphological study, i.e., SEM, was performed using a Carl Zeiss, Supra 40 (New Zealand), while the TEM study was performed using an HR-TEM Tecnai G2 F20 FEI Corporation, the Netherlands, operating at 200 kV. A Thermo 5700 FTIR spectrophotometer (Germany) was used for the characterization of functional groups. An SPR 300 Raman spectrometer having a 532 nm excitation wavelength was used for the Raman study. For pore size measurement and surface area, a BET surface area analyzer, Microtrac Beslorp, having 30% $N_2$/He, $N_2$; 0.15 Mpa; and power of 110/AC230 V, 400 W, and 50/60 Hz was used.

The electrochemical studies (CV, DPV, and EIS) were performed using Autolab (PGSTAT, 302, the Netherlands). A three-electrode assembly, viz., glassy carbon electrode (working electrode, diameter = 3 mm), Pt-foil electrode (counter electrode), and Ag/AgCl (reference electrode), was used for electrochemical studies. The screen-printed carbon electrode (SPCE) (Model number IS-1) was purchased from Palm Sens, the Netherlands, having a reference electrode (area = 1 $mm^2$), a working electrode (diameter = 2 mm), and a counter electrode (area = 3 $mm^2$), and was further modified by the prepared 2D carbon.

## AUTHOR INFORMATION


### Corresponding Authors

**Monika Srivastava** − *School of Materials Science and Technology, Indian Institute of Technology, Banaras Hindu University, Varanasi 221005, India;* orcid.org/0000-0002-4653-9007; Email: monikabhu.srivastava@gmail.com

**Rajiv Prakash** − *School of Materials Science and Technology, Indian Institute of Technology, Banaras Hindu University, Varanasi 221005, India;* orcid.org/0000-0002-6623-522X; Email: rprakash.mst@iitbhu.ac.in

### Authors

**Nikhil** − *School of Materials Science and Technology, Indian Institute of Technology, Banaras Hindu University, Varanasi 221005, India*

**S. K. Srivastava** − *Department of Physics, Institute of Science, Banaras Hindu University, Varanasi 221005, India*

**Amit Srivastava** − *Department of Physics, Institute of Science, Banaras Hindu University, Varanasi 221005, India;* Present Address: Department of Physics, TDPG College, VBS Purvanchal University, Jaunpur - 222001

Complete contact information is available at: https://pubs.acs.org/10.1021/acsomega.1c05800


### Notes

The authors declare no competing financial interest.

## ACKNOWLEDGMENTS

M.S. is thankful to DST, New Delhi, for the WOS fellowship (File no. SR/WOS-A/CS-52/2018). The authors extend their gratitude to Ashish Kumar, SMST, IIT(BHU), for discussion. They also appreciate CIF, IIT (BHU), and DST (TIH) IDAPT for support.

## REFERENCES


(1) Nachman, K. E.; Baron, P. A.; Raber, G.; Francesconi, K. A.; Navas-Acien, A.; Love, D. C. Roxarsone, Inorganic arsenic, and other Arsenic species in chicken: A US-based market basket sample. *Environ. Health Perspect.* **2013**, *121*, 818−824.

(2) Xu, S.; Sabino, F. P.; Janotti, A.; Chase, D. B.; Sparks, D. L.; Rabolt, J. F. Unique surface enhanced raman scattering substrate for the study of arsenic speciation and detection. *J. Phys. Chem. A* **2018**, *122*, 9474−9482.

(3) Stolz, J. F.; Perera, E.; Kilonzo, B.; Kail, B.; Crable, B.; Fisher, E.; Ranganathan, M.; Wormer, L.; Basu, P. Biotransformation of 3-nitro-4-hydroxybenzene arsonic acid (roxarsone) and release of inorganic arsenic by Clostridium species. *Environ. Sci. Technol.* **2007**, *41*, 818−823.

(4) Su, S.; Cao, C.; Zhao, Y.; Dionysiou, D. D. Efficient transformation and elimination of roxarsone and its metabolites by a new $\alpha$-FeOOH@ GCA activating persulfate system under UV irradiation with subsequent As (V) recovery. *Appl. Catal., B* **2019**, *245*, 207−219.

(5) Mangalgiri, K. P.; Adak, A.; Blaney, L. Organoarsenicals in poultry litter: Detection, fate, and toxicity. *Environ. Int.* **2015**, *75*, 68−80.

(6) Chen, C. J.; Kuo, T. L.; Wu, M. M. Arsenic and cancers. *Lancet* **1988**, *331*, 414−415.

(7) Wu, M. M.; Kuo, T. L.; Hwang, Y. H.; Chen, C. J. Dose-response relation between arsenic concentration in well water and mortality from cancers and vascular diseases. *Am. J. Epidemiol.* **1989**, *130*, 1123−1132.

(8) Chen, C. J.; Chen, C. W.; Wu, M. M.; Kuo, T. L. Cancer potential in liver, lung, bladder and kidney due to ingested inorganic arsenic in drinking water. *Br. J. Cancer* **1992**, *66*, 888−892.

(9) Chen, Y.; Graziano, J. H.; Parvez, F.; Liu, M.; Slavkovich, V.; Kalra, T.; Argos, M.; Islam, T.; Ahmed, A.; Rakibuz-Zaman, M.; Hasan, R.; Sarwar, G.; Levy, D.; VanGeen, A.; Ahsan, H. Arsenic exposure from drinking water and mortality from cardiovascular disease in Bangladesh: prospective cohort study. *BMJ* **2011**, *342*, d2431.

(10) Wasserman, G. A.; Liu, X.; Parvez, F.; Ahsan, H.; Factor-Litvak, P.; Kline, J.; Van Geen, A.; Slavkovich, V.; Loiacono, N. J.; Levy, D.; Cheng, Z.; Graziano, J. H. Water arsenic exposure and intellectual function in 6-year-old children in Araihazar, Bangladesh. *Environ. Health Perspect.* **2007**, *115*, 285−289.

(11) Navas-Acien, A.; Silbergeld, E. K.; Pastor-Barriuso, R.; Guallar, E. Arsenic exposure and prevalence of type 2 diabetes in US adults. *J. Am. Med. Assoc.* **2008**, *300*, 814−822.

(12) Ahmad, S. A.; Sayed, M. H.; Barua, S.; Khan, M. H.; Faruquee, M. H.; Jalil, A.; Hadi, S. A.; Talukder, H. K. Arsenic in drinking water and pregnancy outcomes. *Environ. Health Perspect.* **2001**, *109*, 629−631.

(13) Davey, J. C.; Bodwell, J. E.; Gosse, J. A.; Hamilton, J. W. Arsenic as endocrine disruptor: effects of arsenic on estrogen receptor mediated gene expression in vivo and in cell culture. *Toxicol. Sci.* **2007**, *98*, 75−86.

(14) Akilarasan, M.; Kogularasu, S.; Chen, S.-M.; Govindasamy, M.; Chen, T. W.; Ali, A. M.; Al-Hemaid, F.M.A.; Elshikh, M. S.; Farah, M. A. A Green Approach to the Synthesis of Well-Structured Prussian Blue Cubes for the Effective Electrocatalytic Reduction of Antiprotozoal Agent Coccidiostat Nicarbazin. *Electroanalysis* **2018**, *30*, 1669−1677.

(15) Rajaji, U.; Chen, T.-W.; Chinnapaiyana, S.; Chena, S.-M.; Govindasamy, M. Two-dimensional Binary Nanosheets (Bi2Te3@g-

C3N4): Application toward the Electrochemical Detection of Food Toxic Chemical. *Anal. Chim. Acta* **2020**, *1125*, 220−230.
(16) Govindasamy, M.; Wang, S.-F.; Almahri, A.; Rajaji, U. Effects of sonochemical approach and induced contraction of core−shell bismuth sulfide/graphitic carbon nitride as an efficient electrode materials for electrocatalytic detection of antibiotic drug in foodstuffs. *Ultrason. Sonochem.* **2021**, *72*, No. 105445.
(17) Rajaji, U.; Chinnapaiyana, S.; Chen, S.-M.; Mani, G.; Alothman, A. A.; Alshgari, R. A. Bismuth telluride decorated on graphitic carbon nitrides based binary nanosheets: Its application in electrochemical determination of salbutamol (feed additive) in meat samples. *J. Hazard. Mater.* **2021**, *413*, No. 125265.
(18) Ramalingam, M.; Kokulnathan, T.; Tsai1, P.-C.; Arasu, M. V.; Al-Dhabi, N. A.; Prakasham, K.; Ponnusamy, V. K. Ultrasonication-assisted synthesis of gold nanoparticles decorated ultrathin graphitic carbon nitride nanosheets as a highly efficient electrocatalyst for sensitive analysis of caffeic acid in food samples. *Appl. Nanosci.* **2021**, 173.
(19) Govindasamy, M.; Wang, S.-Fu.; Jothiramalingam, R.; Ibrahim, S. N.; Al-lohedan, H. A. A screen-printed electrode modified with tungsten disulfide nanosheets for nanomolar detection of the arsenic drug roxarsone. *Microchim. Acta* **2019**, *186*, No. 420.
(20) Chen, T.-W.; Rajaji, U.; Chena, S.-M.; Chinnapaiyan, S.; Ramalingam, R. J. Facile synthesis of mesoporous WS2 nanorods decorated N-doped RGO network modified electrode as portable electrochemical sensing platform for sensitive detection of toxic antibiotic in biological and pharmaceutical samples. *Ultrason. Sonochem.* **2019**, *56*, 430−436.
(21) Govindasamy, M.; Rajaji, U.; Wanga, S.-F.; Changa, Y.-J.; Ramalingam, R. J.; Chan, C.-Y. Investigation of sonochemically synthesized sphere-like metal tungstate nanocrystals decorated activated carbon sheets network and its application towards highly sensitive detection of arsenic drug in biological samples. *J. Taiwan Inst. Chem. Eng.* **2020**, *114*, 211−219.
(22) Kokulnathan, T.; Jothi, A. I.; Chen, S.-M.; Almutairi, G.; Ahmed, F.; Arshi, N.; AlOtaibi, B. Integrating graphene oxide with magnesium oxide nanoparticles for electrochemical detection of nitrobenzene. *J. Environ. Chem. Eng.* **2021**, *9*, No. 106310.
(23) Kokulnathan, T.; Chen, S.-M. Design and Construction of the Gadolinium Oxide Nanorod-Embedded Graphene Aerogel: A Potential Application for Electrochemical Detection of Postharvest Fungicide. *ACS Appl. Mater. Interfaces* **2020**, *12*, 16216−16226.
(24) Kokulnathan, T.; Wang, T.-J.; Duraisamy, N.; Kumar, E. A.; An-Ni-Sung. Hierarchical nanoarchitecture of zirconium phosphate/graphene oxide: Robust electrochemical platform for detection of fenitrothion. *J. Hazard. Mater.* **2021**, *412*, No. 125257.
(25) Kokulnathan, T.; Anthuvan, A. J.; Chen, S.-M.; Chinnuswamy, V.; Kadirveluc, K. Trace level electrochemical determination of the neurotransmitter dopamine in biological samples based on iron oxide nanoparticle decorated graphene sheets. *Inorg. Chem. Front.* **2018**, *5*, 705.
(26) Tsiamis, A.; Sanchez, F. D.; Hartikainen, N.; Chung, M.; Mitra, S.; Lim, Y. C.; Tan, H. L.; Radacsi, N. Graphene Wrapping of Electrospun Nanofibers for Enhanced Electrochemical Sensing. *ACS Omega* **2021**, *6*, 10568−10577.
(27) Hei, Y.; Li, X.; Zhou, X.; Liu, J.; Hassan, M.; Zhang, S.; Yang, Y.; Bo, X.; Wang, H.-L.; Zhou, M. Cost-effective synthesis of three-dimensional nitrogen-doped nanostructured carbons with hierarchical architectures from the biomass of sea-tangle for the amperometric determination of ascorbic acid. *Anal. Chim. Acta* **2018**, *1029*, 15−23.
(28) Madhu, R.; Karuppiah, C.; Chen, S. M.; Veerakumar, P.; Liu, S. B. Electrochemical detection of 4-nitrophenol based on biomass derived activated carbon. *Anal. Methods* **2014**, *6*, 5274−5528.
(29) Veeramani, V.; Madhu, R.; Chen, S.-M.; Lou, B.-S.; Jayabal, P.; Vasantha, V. S. Biomass-derived functional porous carbons as novel electrode material for the practical detection of biomolecules in human serum and snail hemolymph. *Sci. Rep.* **2015**, *5*, No. 10141.
(30) Zhang, T.; Walawendera, W. P.; Fan, L. T.; Fan, M.; Daugaard, D.; Brown, R. C. Preparation of activated carbon from forest and agricultural residues through CO2 activation. *Chem. Eng. J.* **2004**, *105*, 53−59.
(31) San Miguel, G.; Lambert, S. D.; Graham, N.J.D. Thermal regeneration of granular activated carbons using inert atmospheric conditions. *Environ. Technol.* **2002**, *23*, 1337−1346.
(32) Hamadneh, I.; Abu-Zurayk, R. A.; Al-Dujaili, A. H. Removal of phenolic compounds from aqueous solution using MgCl2-impregnated activated carbons derived from olive husk: the effect of chemical structures. *Water Sci. Technol.* **2020**, *81*, 2351−2367.
(33) Foo, K. Y.; Hameed, B. H. Preparation, characterization and evaluation of adsorptive properties of orange peel based activated carbon via microwave induced $K_2CO_3$ activation. *Bioresour. Technol.* **2012**, *104*, 679−686.
(34) Hai, A.; Bharatha, G.; Ram Babua, K.; Taher, H.; Naushad, Mu.; Banat, F. Date seeds biomass-derived activated carbon for efficient removal of NaCl from saline solution. *Process Saf. Environ. Prot.* **2019**, *129*, 103−111.
(35) Uçar, S.; Erdem, M.; Tay, T.; Karagöz, S. Removal of lead (II) and nickel (II) ions from aqueous solution using activated carbon prepared from rapeseed oil cake by $Na_2CO_3$ activation. *Clean Technol. Environ. Policy* **2015**, *17*, 747−756.
(36) Hu, L.; Zhu, Q.; Wu, Q.; Li, D.; An, Z.; Xu, B. Natural Biomass-Derived Hierarchical Porous Carbon Synthesized by an in Situ Hard Template Coupled with NaOH Activation for Ultrahigh Rate Supercapacitors. *ACS Sustainable Chem. Eng.* **2018**, *6*, 13949−13959.
(37) Uçar, S.; Erdem, M.; Tay, T.; Karagöz, S. Preparation and characterization of activated carbon produced from pomegranate seeds by $ZnCl_2$ activation. *Appl. Surf. Sci.* **2009**, *255*, 8890−8896.
(38) Gehrke, V.; Maron, G. K.; Rodrigues, L.d.S.; Alano, J. H.; Pereira, C.M.P.d.; Orlandi, M. O.; Carreño, N.L.V. Facile preparation of a novel biomass-derived H3PO4 and$Mn(NO_3)_2$ activated carbon from *citrus bergamia* peels for high-performance supercapacitors. *Mater. Today Commun.* **2021**, *26*, No. 101779.
(39) Komal, N. K.; Singh, P. K.; Singh, R.; Shukla, V. K. 'Kusha' (eragrostiscynosuroids): A source of activated carbon for energy storage device. *Mater. Today: Proc.* **2021**, *34*, 702−704.
(40) Gao, Z.; Zhang, Y.; Song, N.; Li, X. Biomass-derived renewable carbon materials for electrochemical energy storage. *Mater. Res. Lett.* **2017**, *5*, 69−88.
(41) Kim, D.; Kim, J. M.; Jeon, Y.; Lee, J.; Oh, J.; Antink, W. H.; Kim, D.; Piao, Y. Novel two-step activation of biomass-derived carbon for highly sensitive electrochemical determination of acetaminophen. *Sens. Actuators, B* **2018**, *259*, 50−58.
(42) Pang, P.; Yan, F.; Chen, M.; Li, H.; Zhang, Y.; Wang, H.; Wu, Z.; Yang, W. Promising biomass-derived activated carbon and gold nanoparticle nanocomposites as a novel electrode material electrochemical detection of rutin. *RSC Adv.* **2016**, *6*, 90446−90454.
(43) Travlou, N. A.; Ushay, C.; Seredych, M.; Rodríguez-Castellón, E.; Bandosz, T. J. Nitrogen-doped activated carbon-based ammonia sensors: effect of specific surface functional groups on carbon electronic properties. *ACS Sens.* **2016**, *1*, 591−599.
(44) Deng, J.; Xiong, T.; Xu, F.; Li, M.; Han, C.; Gong, Y.; Wang, H.; Wang, Y. Inspired by bread leavening: one-pot synthesis of hierarchically porous carbon for supercapacitors. *Green Chem.* **2015**, *17*, 4053−4060.
(45) Madhu, R.; Sankar, K. V.; Chen, S.-M.; Selvan, R. K. Eco-friendly synthesis of activated carbon from dead mango leaves for the ultrahigh sensitive detection of toxic heavy metal ions and energy storage applications. *RSC Adv.* **2014**, *4*, 1225−1233.
(46) Liu, X.; Zhou, Y.; Zhou, W.; Li, L.; Huang, S.; Chen, S. Biomass-derived nitrogen self-doped porous carbon as effective metal-free catalysts for oxygen reduction reaction. *Nanoscale* **2015**, *7*, 6136−6142.
(47) Volpe, R.; Zabaniotou, A. A.; Skoulou, V. Synergistic Effects between Lignin and Cellulose during Pyrolysis of Agricultural Waste. *Energy Fuels* **2018**, *32*, 8420−8430.


https://doi.org/10.1021/acsomega.1c05800
*ACS Omega* 2022, 7, 2908−2917

(48) Garg, U.; Kaur, M. P.; Jawa, G. K.; Sud, D.; Garg, V. K. Removal of cadmium (II) from aqueous solutions by adsorption on agricultural waste biomass. *J. Hazard. Mater.* **2008**, *154*, 1149−1157.
(49) Wan Ngah, W. S.; Hanafiah, M. A. K. M. Removal of heavy metal ions from wastewater by chemically modified plant wastes as adsorbents: A review. *Bioresour. Technol.* **2008**, *99*, 3935−3948.
(50) Yoshizawa, N.; Maruyama, K.; Yamada, Y.; Zielinska-Blajet, M. XRD evaluation of CO2 activation process of coal- and coconut shell-based carbons. *Fuel* **2000**, *79*, 1461−1466.
(51) Ferrari, A. C.; Robertson, J. Interpretation of Raman spectra of disordered and amorphous carbon. *Phys. Rev. B* **2000**, *61*, 14095.
(52) Park, J. S.; Reina, A.; Saito, R.; Kong, J.; Dresselhaus, G.; Dresselhaus, M. S. G′ band Raman spectra of single, double and triple layer graphene. *Carbon* **2009**, *47*, 1303−1310.
(53) Pandey, R.; Prasad, R. L.; Ansari, N. G.; Murthy, R. C. Utilization of NaOH modified Desmostachyabipinnata(Kush Grass) Leaves & Bambusaarundinacea(Bamboo) Leaves for Cd(II) removal from aqueous solution. *J. Environ. Chem. Eng.* **2015**, *3*, 593−601.
(54) Veeramani, V.; Sivakumar, M.; Chen, S.-M.; Madhu, R.; Alamri, H. R.; Alothman, Z. A.; Hossain, M.S.A.; Chen, C.-K.; Yamauchi, Y.; Miyamoto, N.; Wu, K. C-W. Lignocellulosic biomass-derived, graphene sheet like porous activated carbon for electrochemical supercapacitor and catechin sensing. *RSC Adv.* **2017**, *7*, 45668.
(55) Sha, T.; Li, X.; Liu, J.; Sun, M.; Wang, N.; Bo, X.; Guo, Y.; Hu, Z.; Zhou, M. Biomass waste derived carbon nanoballs aggregation networks-based aerogels as electrode material for electrochemical sensing. *Sens. Actuators, B* **2018**, *277*, 195−204.
(56) Bai, L.; Yuan, R.; Chai, Y.; Yuan, Y.; Wang, Y.; Xie, S. Direct electrochemistry and electrocatalysis of glucose oxidase-functionalized bioconjugate as a trace label for ultrasensitive detection of thrombin. *Chem. Commun.* **2012**, *48*, 10972−10974.
(57) Kumar, A.; Pandey, A. C.; Prakash. Electro-oxidation of formic acid using polyindole-$SnO_2$ nanocomposite. *Catal. Sci. Technol.* **2012**, *2*, 2533−2538.
(58) Verma, C. J.; Kumar, A.; Ojha, R. P.; Prakash, R. Au-$V_2O_5$/Polyindole composite: An approach for ORR in different electrolytes. *J. Electroanal. Chem.* **2020**, *861*, 113959−113968.
(59) Yu, X.; Han, X.; Chang, C.; Hu, Y.; Xu, C.; Charles; Fang, S. Corncob-derived activated carbon for roxarsone removal from aqueous solution: isotherms, kinetics, and mechanism. *Environ. Sci. Pollut. Res.* **2020**, *27*, 15785−15797.





https://doi.org/10.1021/acsomega.1c05800
*ACS Omega* 2022, 7, 2908−2917